

1
2
3
4 **Structure-based discovery of CFTR potentiators and inhibitors**
5
6
7

8 Fangyu Liu^{1,2#}, Anat Levit Kaplan^{2#}, Jesper Levring^{1#}, Jürgen Einsiedel^{3#}, Stephanie Tiedt³,
9 Katharina Distler³, Natalie S. Omattage^{1,4}, Ivan S. Kondratov^{5,6}, Yurii S. Moroz^{7,8}, Harlan L.
10 Pietz¹, John J. Irwin², Peter Gmeiner^{3*}, Brian K. Shoichet^{2*}, and Jue Chen^{1,9*}

11 **Affiliations:**

12 1. Laboratory of Membrane Biology and Biophysics, The Rockefeller University, New York, NY
13 10065, USA.

14 2. Dept. of Pharmaceutical Chemistry, University of California, San Francisco, San Francisco
15 CA 94143, USA.

16 3. Dept. of Chemistry and Pharmacy, Medicinal Chemistry, Friedrich-Alexander University
17 Erlangen-Nürnberg, Nikolaus-Fiebiger-Straße 10, D-91058 Erlangen, Germany

18 4. Current address: Department of Infectious Diseases, Genentech, Inc., South San Francisco,
19 CA 94080, USA

20 5. Enamine Ltd. (www.enamine.net), Chervonotkatska Street 78, Kyiv 02094, Ukraine

21 6. V.P. Kukhar Institute of Bioorganic Chemistry & Petrochemistry, National Academy of
22 Sciences of Ukraine, Murmanska Street 1, Kyiv 02660, Ukraine

23 7. Chemspace (www.chem-space.com), Chervonotkatska Street 85, Kyiv 02094, Ukraine

24 8. Taras Shevchenko National University of Kyiv, Volodymyrska Street 60, Kyiv 01601, Ukraine

25 9. Howard Hughes Medical Institute, Chevy Chase, MD 20815, USA.

26 #Contributed equally

27 *co-corresponding authors

28
29
30
31

32 **Abstract**

33 The cystic fibrosis transmembrane conductance regulator (CFTR) is a crucial ion
34 channel whose loss of function leads to cystic fibrosis, while its hyperactivation leads to
35 secretory diarrhea. Small molecules that improve CFTR folding (correctors) or function
36 (potentiators) are clinically available. However, the only potentiator, ivacaftor, has suboptimal
37 pharmacokinetics and inhibitors have yet to be clinically developed. Here we combine molecular
38 docking, electrophysiology, cryo-EM, and medicinal chemistry to identify novel CFTR
39 modulators. We docked ~155 million molecules into the potentiator site on CFTR, synthesized
40 53 test ligands, and used structure-based optimization to identify candidate modulators. This
41 approach uncovered novel mid-nanomolar potentiators as well as inhibitors that bind to the
42 same allosteric site. These molecules represent potential leads for the development of more
43 effective drugs for cystic fibrosis and secretory diarrhea, demonstrating the feasibility of large-
44 scale docking for ion channel drug discovery.

45

46

47

48

49 **Introduction**
50

51 CFTR is an anion channel that is widely expressed in epithelial cells of the lung, intestine,
52 pancreas, and reproductive tract, where it regulates salt and fluid homeostasis¹. Mutations that
53 disrupt CFTR biosynthesis, folding, trafficking, or ion permeation cause cystic fibrosis (CF), a
54 lethal genetic disease with no cure². In addition, excessive activation of CFTR by bacterial
55 pathogens such as *Vibrio cholerae* and enterotoxigenic *Escherichia coli* leads to secretory
56 diarrhea, a major cause of mortality in children under the age of five³. For these reasons,
57 modulators that either up- or downregulate CFTR activity have long been pursued as drug
58 candidates.

59 Although negative CFTR modulators have not yet been advanced to the clinic, there has
60 been considerable progress in the development of positive modulators, including correctors that
61 increase the abundance of CFTR at the cell surface and potentiators that enhance anion flux⁴⁻⁶.
62 Thus far, one potentiator (ivacaftor or VX-770) and three correctors (lumacaftor, tezacaftor, and
63 elexacaftor) have been made available to CF patients². Ivacaftor is prescribed for 178 different
64 CFTR mutations – either singly or in combination with correctors⁷. Although it has certainly
65 improved the health of many CF patients, its physical properties and pharmacokinetics are far
66 from optimal. Ivacaftor is difficult to formulate due to its low water solubility (<0.05 µg/mL; cLogP
67 = 5.6)⁸. Moreover, its bioavailability is highly variable as 99% is bound to plasma proteins^{9,10} and
68 its usage is limited due to side effects, including liver disease and childhood cataracts¹¹.
69 Meanwhile, the high expense of the drug (over \$200,000 per year) is a strain on public health
70 insurance, and puts the drug out of reach of many. Alternative CFTR potentiators, including
71 those inspired by ivacaftor, would therefore be beneficial for CF patients.

72 Ivacaftor's mechanism of action has been studied structurally and functionally.
73 Electrophysiological measurements showed that the drug increases the open probability of
74 many mutants, as well as wild-type (WT), CFTR channels^{12,13}. Cryo-EM structures further
75 revealed that ivacaftor binds to CFTR within the lipid membrane, at a hinge region important for

76 gating¹⁴. The binding-site does not overlap with the positions of disease-causing mutations such
77 as ΔF508 or G551D, indicating that ivacaftor acts as an allosteric modulator. A chemically
78 distinct CFTR potentiator, GLPG1837, binds to the same site on CFTR, indicating that this
79 binding pocket is a hotspot for regulatory ligands. Because the pocket is unique to CFTR, and is
80 not conserved in closely related proteins¹⁵, it is an excellent target for the discovery of CFTR
81 modulators without off-target effects.

82 As a result of recent developments in the use of chemical libraries for molecular docking,
83 it is now feasible to computationally screen large and, more recently, ultra-large chemical
84 libraries to identify potential ligands¹⁶⁻²¹. For example, nanomolar and sub-nanomolar ligands
85 have been identified for dopamine D4, melatonin MT1, sigma2, and alpha2a adrenergic
86 receptors from structure-based virtual screening^{16,19-21}. Thus far, most of the large-scale library
87 screens have focused on enzymes^{16,18} and G protein-coupled receptors (GPCRs)^{17,19-22}. Few
88 studies have been performed on membrane transporters or ion channels. Furthermore, the
89 potentiator-binding site in CFTR is shallow and directly exposed to membrane, posing an extra
90 challenge for virtual screening.

91 In this study, we sought to identify novel CFTR ligands by iterative molecular docking,
92 electrophysiology, cryo-EM, and medicinal chemistry efforts (Figure 1a). The structure of CFTR
93 in complex with ivacaftor was used to computationally dock a large virtual library of diverse
94 chemical scaffolds. Through iterative optimization, we identified a novel potentiator scaffold with
95 mid-nanomolar affinity that is chemically distinct from known CFTR potentiators and that has
96 favorable physical properties and pharmacokinetics. We also discovered modulators that bind to
97 the potentiator site but inhibit CFTR activity, demonstrating that the membrane-exposed
98 allosteric site can be explored to downregulate CFTR activity.

99

100

101

102

103 Results

104

105 Identification of CFTR potentiators

106 Seeking new CFTR modulators, we docked a virtual library of ~155 million tangible
107 “drug-like” molecules (molecular weight 300-350 Da; $\log P \leq 3.5$) from the ZINC database
108 (<http://zinc15.docking.org>)^{23,24} to the CFTR/ivacaftor cryo-EM structure (PDB: 6O2P) using
109 DOCK3.7 (Figure 1a)²⁵. Each molecule was sampled in an average of 421 conformations and
110 3,727 orientations, resulting in over 63 billion complexes being sampled in 76,365 core hours on
111 an in-house cluster. Seeking diverse chemotypes, we clustered the top 100,000 scoring
112 molecules by 2D similarity using ECFP4 fingerprints and a Tanimoto Coefficient (Tc) cutoff of
113 0.5. The top ranked molecules from each cluster (a total of 1,000) were visually inspected to
114 remove molecules that were conformationally strained or had unsatisfied hydrogen bond
115 acceptors or donors. Compounds engaging the key potentiator-binding residues S308, Y304,
116 F312, and F931 (PDB: 6O2P and 6O1V) were prioritized and 58 of those, each from a different
117 chemotype family, were selected for experimental evaluation.

118 Of the 58 prioritized compounds fifty-three were synthesized successfully from the
119 Enamine make-on-demand set, a 91% fulfillment rate; as far as we know, all were new to the
120 planet. They were evaluated for their effects on the CFTR variant found in 90% of CF patients
121 ($\Delta F508$). GLPG1837 was used as a benchmark because ivacaftor has very low solubility²⁶,
122 making it difficult to work with, and studies have shown that GLPG1837, although it was not
123 advanced to the clinic, has a higher cellular efficacy than does ivacaftor for CFTR
124 potentiation^{27,28}. CFTR-mediated ion flux was measured in a bronchial epithelial cell line derived
125 from a patient homozygous for $\Delta F508$ (CFBE41o⁻) using a well-established halide flux assay²⁹.
126 Several of the new compounds potentiated CFTR-mediated ion flux (Extended Figure 1), in
127 particular Z2075279358 ('358), which increased ion flux to an extent close to that of GLPG1837
128 (Figure 1b).

129 Positive hits from this cellular assay were further analyzed electrophysiologically in
130 inside-out membrane patches containing phosphorylated WT CFTR channels (Figure 1c). At a
131 concentration of 5 μ M, 13 compounds increased macroscopic currents by 1.2 to 2.4-fold (Figure
132 1c). The chemotypes of these 13 docking hits were diverse and novel compared to known
133 CFTR potentiators such as GLPG1837 and ivacaftor (Figure 1d). In agreement with our cellular
134 assay, the most efficacious compound was '358, whose efficacy was comparable to that of
135 GLPG1837 (increased macroscopic current by 2.2-fold)^{14,28,30} with an EC₅₀ of 2.2 \pm 0.6 μ M.
136 Furthermore, our large-scale docking screen had a 24% hit rate, further supporting the feasibility
137 of large-scale library screens for identifying novel allosteric ion channel modulators and resulted
138 in candidate potentiators that are effective on both WT and Δ F508 CFTR (Figure 1c and Figure
139 E1).

140

141 **Analog screen to identify additional potentiators**

142 To identify more potent ligands for CFTR, we screened the ZINC15 library for analogs of
143 '358. These were docked into the allosteric potentiator-binding site, and prioritized based on fit.
144 Thirteen high-scoring analogs were selected for synthesis and tested using electrophysiology
145 (Figure 2a). Surprisingly, only one molecule, Z1834339853 ('853), potentiated WT CFTR
146 currents to the same degree as '358 (Figure 2). The other 12 analogs had little or no effect.
147 Concerned by this apparent failure of SAR, we re-examined the structures of the synthesized
148 compounds by detailed NMR spectroscopy. This revealed that both '358 and '853 are
149 regioisomers of the molecules specified in ZINC15 (Figure 2b). The acyl side chains on the
150 exocyclic nitrogens of the indazole rings in both compounds in the ZINC15 database are instead
151 on the cyclic nitrogens (Figure 2b).

152 To analyze how these regioisomeric differences affect binding to CFTR, we compared
153 the docking pose of the synthesized '853 with its regioisomer in ZINC15 (Figure 2c). Like the

154 ZINC15 regioisomer, the synthesized '853 fits well at the potentiator-binding site, forming
155 several identical interactions: its phenyl ring is located in the hydrophobic pocket defined by
156 F312, A436, G438 and R933; the central carbonyl docks to the main chain of F931 via a
157 hydrogen bond; and the indazole ring is poised to stack with F312. The two poses differ in the
158 orientation of the indazole by ~180° but the docking scores are similar: -34.54 kcal/mol for the
159 synthesized compound and -37.13 kcal/mol for the isomer in the ZINC15 database. This
160 suggests that, despite the side chain difference, the synthesized '853 is likely to interact with
161 CFTR at the potentiator-binding site.

162 Because '853 contains a chiral center, the pure enantiomers (S)-'853 and (R)-'853 were
163 synthesized and tested (Figure 2d). Interestingly, although the (S)-enantiomer increased the
164 CFTR currents by 1.5-fold, the (R)-enantiomer decreased the currents by 0.89-fold (Figure 2d).
165 Furthermore, when tested together, the presence of (R)-'853 diminished the potentiating effect
166 of (S)-'853 in a competition assay (Figure 2e), while dose-response curves confirmed greater
167 current flow through CFTR in the presence of (S)-'853 compared to the racemic mixture (Figure
168 2f). Together, these data reveal that the two enantiomers of '853 have opposite functional
169 effects: while (S)-'853 is a potentiator, (R)-'853 is an inhibitor of CFTR.

170
171 **Structural investigation of the '853 binding site**
172

173 To confirm the docking predicted binding pose of '853 and to guide further optimization
174 for affinity and efficacy, we sought to determine the cryo-EM structure of CFTR in complex with
175 '853. Using phosphorylated E1371Q CFTR in the presence of saturating ATP-Mg²⁺ (10 mM), we
176 obtained a 3.8 Å reconstruction which revealed clear density at the allosteric potentiator-binding
177 site (Figure 3a and Figure E2). The shape and size of the density are consistent with the
178 molecular structure of '853 (Figure 3b). Like ivacaftor and GLPG1837, '853 binds to a set of
179 residues near the TM8 hinge region at the protein-membrane interface. Previous mutational
180 scanning experiments identified two polar residues at this location (S308 and Y304) that are

181 critical for ivacaftor and GLPG1837 recognition^{14,30}. Alanine substitution of either residue
182 abolished the potentiating effect of (S)-‘853 in inside-out patches (Figure 3c), confirming that the
183 modulator discovered by molecular docking specifically engages these residues and interacts
184 with CFTR in the same manner as ivacaftor and GLPG1837.

185

186

187 **Structure-based optimization of the CFTR modulators**

188 With the experimental structure of the CFTR/‘853 complex in hand, and given the
189 intriguing difference between (S)-‘853 and (R)-‘853, we carried out further optimization to
190 identify additional potentiators and inhibitors. We used the following medicinal chemistry
191 strategies to synthesize multiple classes of ‘853 analogs (Figure 4a and Extended Figure 3): (1)
192 replacing the fluorine with a larger side chain bearing either hydrogen-bond donor or acceptor
193 functionality (Y); (2) removing the linker methyl or replacing it with a bulkier group (Z), or
194 replacing the linker oxygen with a methylene group (W); (3) removing or modifying the amino
195 group’s hydrogen donor functionality (X); (4) replacing the terminal phenyl ring with aromatic
196 moieties, such as benzofuran or naphthalene, to improve stacking with F312, F316 and F931 or
197 adding side chains to the distal phenyl ring (ARYL).

198

199 Each of the designed compounds was docked into the potentiator-binding site *in silico*,
200 and a total of 39 compounds were chosen for synthesis based on their docking score. The
201 efficacies of the synthesized analogs were determined by patch clamp experiments, revealing a
202 continuum of CFTR modulation from inhibition to potentiation (Figure 4b). The most efficacious
203 analogs, which strongly potentiated CFTR, were the ones in which the para-position in the distal
204 phenyl ring was halogenated and/or the indazole fluorine was replaced by a hydroxyl group. The
205 first modification improved the non-polar complementarity in a hydrophobic subsite of the
206 potentiator-binding pocket (Extended Figure 4, right panel), while the replacement of the (S)-

207 '853 indazole fluorine with a polar group is predicted to form a hydrogen bond with Q237 and
208 S308 (Figure 4b and Figure E3, Figure 4). Three of the most potent potentiators, I1421, I1408,
209 and (S)-SX-263, increased currents through WT CFTR with EC_{50} values of 64 ± 25 nM, 93 ± 42
210 nM and 136 ± 60 nM, respectively (Figure 4c).

211 Of the 39 analogs tested, several were found to inhibit WT CFTR (Figure 4d and
212 Extended Figure 3), including I1412. This compound is an (R)-enantiomer of the potentiator
213 I1409, providing a second example of (S)- and (R)-enantiomers being positive and negative
214 allosteric modulators, respectively (Figure 4b). The most potent inhibitors in this series inhibited
215 WT CFTR with IC_{50} values of 21 ± 3 μ M (I1412) and 41 ± 17 μ M (I1422) (Figure 4d). Similar to
216 the potentiator (S)-'853, single alanine substitutions of either of the binding site residues Y304
217 or S308 eliminated the activity of I1412 (Figure 4d). This medicinal chemistry approach thus led
218 to the identification of a novel potentiator (I1421) with a 30-fold greater potency than (S)-'853, as
219 well as negative modulators that bind to the same site on CFTR.

220

221 **I1421 can rescue multiple CF-causing mutants**

222 Finally, we asked whether the strongest potentiator, I1421, could increase the activity of
223 various disease-causing CFTR mutants. Clones carrying ten of these mutations, distributed at
224 different positions in CFTR, were tested using patch-clamp electrophysiology (Figure 5a). The
225 predominant CF mutation, Δ F508, is defective in both folding and gating. Newly synthesized
226 Δ F508 CFTR is largely retained in the endoplasmic reticulum³¹ and the few channels that reach
227 the plasma membrane exhibit little activity^{32,33}. I1421 strongly increased currents through Δ F508,
228 indicating that, similar to ivacaftor, it could be used to rescue Δ F508 if used in combination with
229 correctors (Figure 5b, c). Approximately 4% of CF patients carry the G551D mutant, which is
230 expressed on the cell surface but has severe gating defects³⁴. In inside-out membrane patches,
231 I1421 increased the activity of G551D by 25-fold (Figure 5b, c). Potentiation of the other eight
232 mutations by I1421 was also comparable to that of GLPG1837 (Figure 5c). These data indicate

233 that I1421 is a strong potentiator that allosterically activates a wide range of CF-causing
234 mutants.

235

236 Given these promising results, we investigated the pharmacokinetics of I1421 in
237 C57BL/6 mice following single 10 mg/kg doses administrated by intraperitoneal (IP), oral, or
238 subcutaneous routes (Figure 5d, e). As expected from its cLogP value of 2.5, I1421 was readily
239 formulated in a standard vehicle comprising 10% N-Methyl-Pyrrolidone (NMP), 5% solutol HS-
240 15, and 85% saline. The maximum plasma concentrations (C_{max}), observed 15 minutes after IP
241 and oral administration, were 7.4 μ M and 3.4 μ M, respectively, indicating rapid absorption of the
242 compound. Plasma levels following IP administration were higher than the other two routes of
243 administration, as indicated by the areas under the respective plasma concentration curves
244 (AUC) (Figure 5d, e). To determine oral bioavailability, I1421 was intravenously (IV) injected
245 into a group of nine mice at a dose of 3 mg/kg. Comparison of plasma levels from oral versus IV
246 injection yielded a bioavailability of 60%, an encouraging value given that the compound was
247 not subject to special formulation. In contrast, the low solubility of ivacaftor²⁶ has precluded
248 creation of an IV formulation, preventing determination of its oral bioavailability. Low solubility
249 may also affect the non-linear relationship between dose and maximum concentration *in vivo*,
250 causing ivacaftor's C_{max} to plateau with increasing dose^{35,36}, even after extensive formulation
251 optimization. These factors, along with the strong effect of fat-containing food on absorption⁹,
252 may contribute to the variable effects of ivacaftor.

253 Importantly, I1421 and other molecules in this series are not clinical candidates, have
254 not been optimized for pharmacokinetics, and retain liabilities such as a short oral $T_{1/2}$ of 75
255 minutes. Nevertheless, these results support the notion that a structure-based approach to
256 CFTR drug discovery can identify molecules with improved physical properties, easier
257 formulation, and improved pharmacokinetics.

258

259

260 **Discussion**

261 Large library docking has been a disruptive innovation in structure-based ligand
262 discovery, in particular for GPCRs^{17,19-22} and enzymes^{16,18}. However, such screens, and more
263 broadly structure-based design and discovery, are much less prominent for ion channels. In this
264 study, large library docking against the potentiator-binding site of CFTR revealed novel
265 potentiators and inhibitors with chemotypes unrelated to known modulators and with better
266 physical properties than the widely used drug ivacaftor. Several aspects of this study are worth
267 highlighting. First, despite the shallow, membrane-exposed binding pocket, the docking hit rate
268 (number of molecules active/number experimentally tested) was substantial at 24%. Second,
269 despite their chemical novelty and dissimilarity to previously known modulators, potent
270 potentiators were still found. For example, I1421 had a potency comparable to that of
271 GLPG1837 for all ten CF-causing mutants tested. Third, the molecules that we discovered were
272 substantially more polar than the only FDA-approved potentiating drug, ivacaftor, conferring
273 potential benefits to their behavior *in vivo*. This was borne out in preliminary pharmacokinetic
274 experiments in which I1421 was readily formulated for oral and IV delivery using widely used
275 excipients, resulting in substantial exposure upon oral dosing and a high oral bioavailability of
276 60%. The good physical properties of this family, and their apparently favorable
277 pharmacokinetics, provide the freedom for further development and optimization. The structure-
278 based approach described here provides multiple points of departure for drug leads for a
279 disease whose treatment remains out of reach for many, and expensive for all. Finally, our study
280 revealed that the allosteric binding site on CFTR can be used to discover not only potentiators
281 but also inhibitors. Such inhibitors may serve as starting points for the development of
282 treatments for secretory diarrhea, the second leading cause of death in children worldwide.

283 We also wish to draw attention to certain caveats. In particular, we have not tested our
284 potentiators in an animal model, mainly due to the lack of a model system that fully recapitulates
285 the symptoms of human CF³⁷. Indeed, CF drug discovery, including the development of
286 ivacaftor, has historically relied on *in vitro* model systems, some of which were used here. In
287 addition, it is important to note that the promising pharmacokinetics of compounds like I1421 are
288 distinct from their pharmacodynamics, so must be viewed cautiously. Moreover, although
289 solubility and oral bioavailability are encouraging, these molecules remain far from optimized
290 and are currently no more than leads. In our docking experiments, the fact that the most potent
291 initial hit represented a different regioisomer to our intended compound tempers the success of
292 the method, even though the two regioisomers occupy similar poses in the binding site and
293 achieve similar docking scores. Finally, although the initial hits sampled a broad range of
294 chemotypes (Figure 1), their potentiating potencies were modest and have yet to be followed up.

295 Regardless of these caveats, we have made a number of important observations in this
296 study. By docking a large virtual library against the structure of CFTR, we have uncovered 13
297 diverse chemical scaffolds that are topologically distinct from known ligands and have favorable
298 physical properties. This wide range of chemotypes holds great promise for new drug discovery
299 efforts against this crucial target. Indeed, the chemical novelty of these compounds supported
300 our discovery of CFTR inhibitors that likely bind to the same allosteric site, and which have the
301 potential to become lead molecules for the treatment of secretory diarrhea. By determining the
302 structure of one of the new ligands in complex with CFTR, we have provided a template for
303 further optimization of this series and for other drug discovery efforts. Encouragingly, the
304 beneficial physical properties of I1421 resulted in favorable pharmacokinetics during animal
305 dosing. In conclusion, our study has revealed that combining structural biology with exploration
306 of a large chemical space can reveal new lead molecules for what remains a crucial drug target
307 for CF and secretory diarrhea.

308

309 **Methods**

310

311 **Ultra-large scale virtual ligand screening**

312 The recently determined CFTR/ivacaftor cryo-EM structure (PDB: 6O2P;¹⁴) was used to
313 prospectively screen ~155 million “lead-like” molecules (molecular weight 300-350 Da and logP
314 ≤ 3.5), from the ZINC15 database (<http://zinc15.docking.org/>²⁴), using DOCK3.7²⁵. DOCK3.7 fits
315 pregenerated flexible ligands into a small molecule binding site by superimposing atoms of each
316 molecule on local hot spots in the site (“matching spheres”), representing favorable positions for
317 individual ligand atoms. Here, 45 matching spheres were used, drawn from the experimentally
318 determined pose of ivacaftor. The resulting docked ligand poses were scored by summing the
319 channel–ligand electrostatics and van der Waals interaction energies and corrected for context-
320 dependent ligand desolvation^{38,39}. Channel structures were protonated using Reduce⁴⁰. Partial
321 charges from the united-atom AMBER force field were used for all channel atoms⁴¹. Potential
322 energy grids for the different energy terms of the scoring function were precalculated based on
323 the AMBER potential⁴¹ for the van der Waals term and the Poisson–Boltzmann method
324 QNIFFT73^{42,43}, for electrostatics. Context-dependent ligand desolvation was calculated using an
325 adaptation of the generalized-Born method³⁸. Ligands were protonated with Marvin (version
326 15.11.23.0, ChemAxon, 2015; <https://www.chemaxon.com>), at pH 7.4. Each protomer was
327 rendered into 3D using Corina (v.3.6.0026, Molecular Networks GmbH; <https://www.mn->
328 [am.com/products/corina](https://www.mn-am.com/products/corina)) and conformationally sampled using Omega (v.2.5.1.4, OpenEye
329 Scientific Software; <https://www.eyesopen.com/omega>). Ligand atomic charges and initial
330 desolvation energies were calculated as described²⁴. In the docking screen, each library
331 molecule was sampled in about 3,727 orientations and, on average, 421 conformations. The
332 best scoring configuration for each docked molecule was relaxed by rigid-body minimization.
333 Overall, over 63 billion complexes were sampled and scored; this took 76,365 core hours–
334 spread over 1000 cores, or slightly more than 3 days.

335

336 To identify novel and diverse chemotypes, the top 100,000 scoring molecules were clustered by
337 2D similarity using ECFP4 fingerprints and a Tanimoto Coefficient (Tc) cutoff of 0.5. The top
338 ranked 1,000 cluster heads were visually inspected in their docked poses to remove molecules
339 that are conformationally strained or with unsatisfied hydrogen-bond acceptors or donors.
340 Topologically diverse molecules that adopted favorable geometries and formed specific
341 interactions with the key potentiator-binding residues S308, Y304, F312, and F931 (PDB: 6O2P
342 and 6O1V), were prioritized from among the top 1000 docking-ranked molecules.

343

344 Ultimately, 58 compounds, each from a different chemotype family, were selected for
345 experimental evaluation.

346

347 **Synthesis of molecules**

348 Fifty-three molecules prioritized for purchasing were synthesized by Enamine for a total
349 fulfilment rate of 91%. Compounds were sourced from the Enamine REAL database
350 (<https://enamine.net/compound-collections/real-compounds>). The purities of active molecules
351 synthesized by Enamine were at least 90% and typically above 95%. For compounds
352 synthesized in house purities were at least 95%. The detailed chemical synthesis can be found
353 in the Chemical Synthesis and analytical investigations section.

354

355 **Hit Optimization**

356 Potential analogs of the hit compound Z2075279358 were identified through a combination of
357 similarity and substructure searches of the ZINC database²⁴. Potential analogs were docked to
358 the CFTR small molecule binding site using DOCK3.7³⁸. As was true in the primary screen, the
359 resulting docked poses were manually evaluated for specific interactions and compatibility with
360 the site, and prioritized analogs were acquired and tested experimentally.

361

362 **Chemical Synthesis and analytical investigations**

363 The library from Enamine were synthesized taking advantage of synthesis protocols previously
364 published (also see below)^{44,45,46}.

365 The synthetic procedures for pure enantiomers of '853 and its analogs were depicted in
366 supplementary information. Furthermore, the ¹H- and ¹³C-NMR spectra, the HPLC-
367 chromatograms demonstrating purity > 95% and proving optical purity are included.

368

369 **Pharmacokinetic Study**

370 Pharmacokinetic experiments of I1421 were performed by Sai Life Sciences (Hyderabad, India)
371 at an AAALAC accredited facility in accordance with the Sai Study Protocol SAIDMPK/PK-22-
372 12-1306 and PK-22-11-1117. International guidelines for animal experiments were followed.

373 Plasma pharmacokinetics of compound I1421 was measured after a single 10 mg/kg dose,
374 administered intraperitoneal (IP), per-orally (PO) or subcutaneously (SC). Plasma samples were
375 also collected from mice after a single 3 mg/kg intravenous (IV) dose injection to determine oral
376 bioavailability. Both doses were formulated in 10% NMP:5% Solutol HS-15: 85% saline (v/v/v).

377 Testing was done in healthy male C57BL/6 mice (8-10 weeks old) weighing between 25 ± 5 g
378 (procured from Global, India). Three mice were housed in each cage. Temperature and humidity
379 were maintained at 22 ± 3 °C and 30-70%, respectively and illumination was controlled to give a
380 sequence of 12 h light and 12 h dark cycle. Temperature and humidity were recorded by an
381 auto-controlled data logger system. All animals were provided laboratory rodent diet (Envigo
382 Research private Ltd, Hyderabad). Reverse osmosis water treated with ultraviolet light was
383 provided *ad libitum*.

384 For the 10 mg/kg (IP, PO and SC) study, a total of twenty-seven mice were used. Animals in
385 Group 1 (n=9) were administered IP, animals in Group 2 (n=9) were administered PO and
386 animals in Group 3 (n=9) were administered SC with solution formulation of I1421. For the 3

387 mg/kg (IV) study, animals in Group 1 (n=9) were administered IV with the same solution
388 formulation. Blood samples (approximately 60 μ L) were collected from the retro orbital plexus of
389 a set of three mice at 0.083, 0.25, 0.5, 1, 2, 4, 6, 8 and 24 h. Immediately after blood collection,
390 plasma was harvested by centrifugation at 10000 rpm, 10 min at 4 $^{\circ}$ C and samples were stored
391 at -70 \pm 10 $^{\circ}$ C until bioanalysis. All samples were processed for analysis by protein precipitation
392 method and analyzed with fit-for-purpose LC-MS/MS method (LLOQ = 1.02 ng/mL for plasma).
393 The pharmacokinetic parameters were estimated using non-compartmental analysis tool of
394 Phoenix® WinNonlin software (Ver 8.3).

395
396 Sample Extraction Procedure: 10 μ L of study sample plasma or spiked plasma calibration
397 standard was added to individual pre-labeled micro-centrifuge tubes followed by 100 μ L of
398 internal standard prepared in Acetonitrile (Cetirizine, 50 ng/mL) except for a blank, where 100 μ L
399 of Acetonitrile was added. Samples were vortexed for 5 minutes. Samples were centrifuged for
400 10 minutes at a speed of 4000 rpm at 4 $^{\circ}$ C. Following centrifugation, 200 μ L of clear
401 supernatant was transferred into 96 well plates and analyzed using LC-MS/MS.

402
403 Data Analysis: Peak plasma concentration (C_{max}) and time for the peak plasma concentration
404 (T_{max}) were the observed values. The areas under the concentration time curve (AUC_{last} and
405 AUC_{inf}) were calculated by the linear trapezoidal rule. The terminal elimination rate constant, ke
406 was determined by regression analysis of the linear terminal portion of the log plasma
407 concentration-time curve. The terminal half-life ($T_{1/2}$) was estimated at 0.693/ ke . Mean, SD and
408 %CV was calculated for each analyte. The bioavailability is calculated by $\%F = \frac{AUC_{oral}}{AUC_{IV}} \times$
409 $\frac{Dose_{IV}}{Dose_{oral}} \times 100\%$, with AUC_{oral} as 1,211 h*ng/ml and AUC_{IV} as 610 h*ng/ml with 10 mg/kg
410 and 3 mg/kg dosing respectively.

411

412 **Cell culture**

413 Sf9 cells were cultured in Sf-900 II SFM medium (GIBCO) supplemented with 5% (v/v) fetal
414 bovine serum (FBS) and 1% (v/v) Antibiotic-Antimycotic. HEK293S GnT^I cells were cultured in
415 Freestyle 293 (GIBCO) supplemented with 2% (v/v) FBS and 1% (v/v) Antibiotic-Antimycotic.
416 Chinese hamster ovary (CHO) cells were cultured in DMEM-F12 (ATCC) supplemented with 10%
417 (v/v) FBS and 1% (v/v) Antibiotic-Antimycotic. CFBE41o- cells expressing F508del-CFTR and
418 the fluorescent protein eYFP-H148Q/I152L/F46L were cultured in MEM-alpha with 10% (v/v)
419 FBS, 1% (v/v) Pen-Strep, 2 mg/mL Puromycin and 0.75 mg/mL G418.

420

421 **Mutagenesis**

422 All mutations were introduced using QuikChange Site-Directed Mutagenesis System
423 (Stratagene).

424

425 **Protein expression and purification**

426 CFTR E1317Q was expressed and purified as described ^{15,47}. In summary, bacmids carrying
427 CFTR E1317Q construct were generated in *E. Coli* DH10Bac cells (Invitrogen). Recombinant
428 baculoviruses were produced and amplified in Sf9 cells. Proteins were expressed in HEK293S
429 GnT^I cells infected with 10% (v/v) baculovirus at a density of 3x10⁶ cells/ml. Cells were induced
430 with 10 mM sodium butyrate 12 hours after infection and cultured at 30 °C for another 48 hours
431 before harvesting.

432

433 For protein purification, cell membranes were solubilized in buffer containing 1.25% (w/v) 2,2-
434 didecylpropane-1,3-bis-β-D-maltopyranoside (LMNG) and 0.25% (w/v) cholesteryl
435 hemisuccinate (CHS). Protein was purified via its C-terminal green fluorescence protein (GFP)
436 tag using GFP nanobody-coupled Sepharose beads (GE Healthcare) and eluted by removing

437 the GFP tag with PreScission Protease. The sample was phosphorylated using protein kinase A
438 (NEB) and then further purified on size exclusion chromatography.

439

440 **EM data acquisition**

441 The phosphorylated E1371Q sample (5.5 mg/mL in 0.06% (w/v) digitonin) was incubated with
442 10 mM ATP and MgCl₂ plus 200 μM Z1834339853 on ice for 15 min. 3 mM fluorinated Fos-
443 choline-8 was added to the sample immediately before freezing on to Quantifoil R1.2/1.3 400
444 mesh Au grids using a Vitrobot Mark IV (FEI). EM images were collected on a 300 kV Titian
445 Krios (FEI) with a K2 Summit detector (Gatan) in super-resolution mode using SerialEM. The
446 defocus ranged from 1 to 2.5 μm and the dose rate was 8 e-/pixel/sec. The data were collected
447 in two sessions, with 3,088 and 3,879 movies collected.

448

449 **EM data processing**

450 The images of the CFTR/Z1834339853 dataset were first corrected for gain reference and
451 binned by 2 to obtain a physical pixel size of 1.03 Å. Beam-induced sample motion was
452 corrected using MotionCor2 ⁴⁸. CTF estimation was performed using Gctf ⁴⁹. Particles were
453 automatically picked by Relion ⁵⁰.

454

455 Two datasets were collected. For the first dataset, a total number of 1,346,123 particles were
456 extracted from 3,879 movies and were subjected to two rounds of 2D classification. 267,967
457 particles and 190,253 particles were selected and combined. Duplicated molecules were
458 removed to yield 313,972 particles for 3D classification. The best classes from the last 4
459 iterations of 3D classification were combined; duplicated particles were removed to yield
460 254,123 particles. For further classification, the best map from 3D classification was low pass
461 filtered to 8, 16, 24, 32, 40, 48 Å and used as reference maps. Local searches were performed
462 at 7.5 and 3.75 degrees for 25 iterations respectively. Thorough searches were done by setting

463 –maxsig 5. Such classification led to 6 classes, with the best class including 40% of the 254,123
464 particles and having a resolution of 7.92 Å. The best class (102,891 particles) was polished and
465 refined to yield a reconstruction of 4.1 Å. Postprocessing did not improve the resolution further.
466 In the second dataset, a total number of 801,032 particles from 3,088 movies were used for 2D
467 classification, and subsequently 602,374 particles were used for 3D classification in RELION2⁵¹.
468 3D classification yielded a best class with 200,815 particles. These particles were further
469 classified with the same six reference models as the previous dataset. The best class contained
470 106,212 particles and were polished and refined to a 4.9 Å map. The polished particles from the
471 two datasets were combined and imported to cryosparc for non-uniform refinement to yield a
472 final map of 3.8 Å.

473

474 **Model building and refinement**

475 The model building and refinement of CFTR were carried out as described¹⁵. In brief, the data
476 was randomly split into two halves, one half for model building and refinement (working set) and
477 the other half for validation (free set). The model was built in Coot⁵² and refined in reciprocal
478 space with Refmac^{53,54}. MolProbity^{55,56} was used for geometry validation and Blocres⁵⁷ was
479 used for local resolution estimation. Final structures contain residues 1–390 of transmembrane
480 domain 1 (TMD1); 391–409, 437–637 of nucleotide binding domain (NBD1); 845–889, 900–
481 1173 of transmembrane domain 2 (TMD2); 1202–1451 of nucleotide binding domain 2 (NBD2);
482 and 17 residues of R domain (built as alanines). Figures were generated with PyMOL and
483 Chimera⁵⁸.

484

485 **Inside-out patch clamp recording**

486 All CFTR constructs used for electrophysiology were cloned into the BacMam expression vector.
487 A GFP tag was fused to the C-terminus of CFTR for visualization of transfected cells. Chinese
488 hamster ovary (CHO) cells were plated at 0.4x10⁶ cells per 35-mm dish (Falcon) 12 hours

489 before the transfection. For each dish, cells were transfected with 1 μ g BacMam plasmids using
490 Lipofectamine 3000 (Invitrogen) in Opti-MEM media (Gibco). After 12 hours of transfection,
491 media was exchanged to DMEM: F12 (ATCC) supplemented with 2% (v/v) FBS and the cells
492 were incubated at 30 °C for 2 days before recording.

493

494 Macroscopic currents were recorded in inside-out membrane patches excised from CHO cells,
495 using buffer compositions, and recording parameters as described ²⁸. The culture media were
496 first changed to a bath solution consisting of 145 mM NaCl, 2 mM MgCl₂, 5 mM KCl, 1 mM
497 CaCl₂, 5 mM glucose, 5 mM HEPES, and 20 mM sucrose, pH 7.4 with NaOH. The pipette
498 solution contained 140 mM *N*-Methyl-D-glucamine (NMDG), 5 mM CaCl₂, 2 mM MgCl₂, and 10
499 mM HEPES (pH 7.4 with HCl). The perfusion solution contained 150 mM NMDG, 2 mM MgCl₂,
500 1 mM CaCl₂, 10 mM EGTA, and 8 mM Tris (pH 7.4 with HCl). Borosilicate micropipettes (OD 1.5
501 mm, ID 0.86 mm, Sutter) were pulled to 2-5 M Ω resistance. After a gigaseal was formed, inside-
502 out patches were excised and exposed to 25 units/ml bovine heart PKA (Sigma-Aldrich, P2645)
503 and 3 mM ATP to phosphorylate CFTR. Currents were recorded at -30 mV and 25 °C using an
504 Axopatch 200B amplifier, a Digidata 1550 digitizer and pCLAMP software (Molecular Devices).
505 The recordings were low-pass filtered at 1 kHz and sampled at 20 kHz. All displayed recordings
506 were further low-pass filtered at 100 Hz. Data were analyzed with Clampfit, GraphPad Prism,
507 and OriginPro. The effect of the compounds were reported as normalized current which was
508 defined as the current level after application of the tested compound divided by the current level
509 before application of the compound.

510

511 **YFP fluorescent assay**

512 The experiments were performed as described in the literature⁵⁹. In brief, 50,000 cells (not
513 cultured beyond passage 10) were seeded per well in 96-well plates (GBO 655866) 48 hours
514 before the start of assay, and incubated at 37 °C. 24 hours before the start of the assay, the

515 CFTR corrector lumacaftor was added at 1 μ M in a final culture volume of 200 μ L. The plates
516 were incubated at 30 °C for 24 hours. On the day of experiments, the cells were first washed
517 three times with 200 μ L PBS (HyClone SH30264.02), and then incubated with 20 μ M forskolin
518 and 1 μ M test compound for 25 minutes in a 60 μ L total volume. The plate was then transferred
519 to a microplate reader for a 14 second fluorescence reading, split into a 2 second baseline
520 reading, rapid injection of 165 μ L iodide containing solution (PBS with 137 mM Cl⁻ replaced by I⁻
521), and then a 12 second reading. Data were normalized to initial background-subtracted
522 fluorescence. I⁻ influx rate was determined by fitting the final 11 seconds of data for each well
523 with an exponential function to extrapolate the initial rate of fluorescence quenching (dF/dt).
524 Relative potentiation is defined as the initial rate of fluorescence decay with test compound
525 divided by the initial rate of fluorescence decay without test compound.

526 **Quantification and Statistical Analysis**

527 GraphPad Prism 9 was used to fit the dose response curves of CFTR potentiators and inhibitors
528 and to calculate EC₅₀s. Statistical significance was calculated by two-tailed Student's t-test in
529 Prism 9.

530

531 **Data availability:** All data are available in the main text, the supplementary materials, the listed
532 Protein Data Bank (PDB) file and the Electron Microscopy Data Bank (EMDB) files. The 3D
533 cryo-EM density map of CFTR-'853 complex generated in this study has been deposited with
534 accession code EMD-40207. The coordinate of CFTR-'853 complex has been deposited with
535 PDB accession code 8GLS. The identities of compounds docked in this study are freely
536 available from the ZINC15 and ZINC20 databases
537 (<https://zinc15.docking.org/> and <https://zinc20.docking.org/>), and active compounds may be
538 purchased from Enamine. DOCK3.7 is freely available for noncommercial research

539 (<https://dock.compbio.ucsf.edu/DOCK3.7/>). A web-based version is freely available to all
540 (<https://blaster.docking.org/>).

541

542

543

544

545 **References**

546 1 Cutting, G. R. Cystic fibrosis genetics: from molecular understanding to clinical
547 application. *Nat Rev Genet* **16**, 45-56, doi:10.1038/nrg3849 (2015).

548 2 Jaques, R., Shakeel, A. & Hoyle, C. Novel therapeutic approaches for the management
549 of cystic fibrosis. *Multidiscip Respir Med* **15**, 690, doi:10.4081/mrm.2020.690 (2020).

550 3 Thiagarajah, J. R. & Verkman, A. S. CFTR inhibitors for treating diarrheal disease. *Clin
551 Pharmacol Ther* **92**, 287-290, doi:10.1038/clpt.2012.114 (2012).

552 4 Hadida, S. et al. Discovery of N-(2,4-di-tert-butyl-5-hydroxyphenyl)-4-oxo-1,4-
553 dihydroquinoline-3-carboxamide (VX-770, ivacaftor), a potent and orally bioavailable
554 CFTR potentiator. *J Med Chem* **57**, 9776-9795, doi:10.1021/jm5012808 (2014).

555 5 Middleton, P. G. et al. Elexacaftor-Tezacaftor-Ivacaftor for Cystic Fibrosis with a Single
556 Phe508del Allele. *N Engl J Med* **381**, 1809-1819, doi:10.1056/NEJMoa1908639 (2019).

557 6 Ramsey, B. W. et al. A CFTR potentiator in patients with cystic fibrosis and the G551D
558 mutation. *N Engl J Med* **365**, 1663-1672, doi:10.1056/NEJMoa1105185 (2011).

559 7 Balfour-Lynn, I. M. & King, J. A. CFTR modulator therapies - Effect on life expectancy in
560 people with cystic fibrosis. *Paediatr Respir Rev* **42**, 3-8, doi:10.1016/j.prrv.2020.05.002
561 (2022).

562 8 Chin, S. et al. Lipophilicity of the Cystic Fibrosis Drug, Ivacaftor (VX-770), and Its
563 Destabilizing Effect on the Major CF-causing Mutation: F508del. *Mol Pharmacol* **94**, 917-
564 925, doi:10.1124/mol.118.112177 (2018).

565 9 McColley, S. A. A safety evaluation of ivacaftor for the treatment of cystic fibrosis. *Expert
566 Opin Drug Saf* **15**, 709-715, doi:10.1517/14740338.2016.1165666 (2016).

567 10 Wainwright, C. E. Ivacaftor for patients with cystic fibrosis. *Expert Rev Respir Med* **8**,
568 533-538, doi:10.1586/17476348.2014.951333 (2014).

569 11 Talamo Guevara, M. & McColley, S. A. The safety of lumacaftor and ivacaftor for the
570 treatment of cystic fibrosis. *Expert Opin Drug Saf* **16**, 1305-1311,
571 doi:10.1080/14740338.2017.1372419 (2017).

572 12 Yu, H. et al. Ivacaftor potentiation of multiple CFTR channels with gating mutations. *J
573 Cyst Fibros* **11**, 237-245, doi:10.1016/j.jcf.2011.12.005 (2012).

574 13 Van Goor, F. et al. Rescue of CF airway epithelial cell function in vitro by a CFTR
575 potentiator, VX-770. *Proc Natl Acad Sci U S A* **106**, 18825-18830,
576 doi:10.1073/pnas.0904709106 (2009).

577 14 Liu, F. et al. Structural identification of a hotspot on CFTR for potentiation. *Science* **364**,
578 1184-1188, doi:10.1126/science.aaw7611 (2019).

579 15 Zhang, Z. & Chen, J. Atomic Structure of the Cystic Fibrosis Transmembrane
580 Conductance Regulator. *Cell* **167**, 1586-1597 e1589, doi:10.1016/j.cell.2016.11.014
581 (2016).

582 16 Lyu, J. et al. Ultra-large library docking for discovering new chemotypes. *Nature* **566**,
583 224-229, doi:10.1038/s41586-019-0917-9 (2019).

584 17 Stein, R. M. et al. Virtual discovery of melatonin receptor ligands to modulate circadian
585 rhythms. *Nature* **579**, 609-614, doi:10.1038/s41586-020-2027-0 (2020).

586 18 Gorgulla, C. et al. An open-source drug discovery platform enables ultra-large virtual
587 screens. *Nature* **580**, 663-668, doi:10.1038/s41586-020-2117-z (2020).

588 19 Alon, A. et al. Structures of the sigma(2) receptor enable docking for bioactive ligand
589 discovery. *Nature* **600**, 759-764, doi:10.1038/s41586-021-04175-x (2021).

590 20 Fink, E. A. et al. Structure-based discovery of nonopioid analgesics acting through the
591 alpha(2A)-adrenergic receptor. *Science* **377**, eabn7065, doi:10.1126/science.abn7065
592 (2022).

593 21 Sadybekov, A. A. et al. Synthon-based ligand discovery in virtual libraries of over 11
594 billion compounds. *Nature* **601**, 452-459, doi:10.1038/s41586-021-04220-9 (2022).

595 22 Kaplan, A. L. *et al.* Bespoke library docking for 5-HT(2A) receptor agonists with
596 antidepressant activity. *Nature* **610**, 582-591, doi:10.1038/s41586-022-05258-z (2022).

597 23 Irwin, J. J., Sterling, T., Mysinger, M. M., Bolstad, E. S. & Coleman, R. G. ZINC: a free
598 tool to discover chemistry for biology. *J Chem Inf Model* **52**, 1757-1768,
599 doi:10.1021/ci3001277 (2012).

600 24 Sterling, T. & Irwin, J. J. ZINC 15--Ligand Discovery for Everyone. *J Chem Inf Model* **55**,
601 2324-2337, doi:10.1021/acs.jcim.5b00559 (2015).

602 25 Coleman, R. G., Carchia, M., Sterling, T., Irwin, J. J. & Shoichet, B. K. Ligand pose and
603 orientational sampling in molecular docking. *PLoS One* **8**, e75992,
604 doi:10.1371/journal.pone.0075992 (2013).

605 26 Csanady, L. & Torocsik, B. Cystic fibrosis drug ivacaftor stimulates CFTR channels at
606 picomolar concentrations. *Elife* **8**, doi:10.7554/elife.46450 (2019).

607 27 Van der Plas, S. E. *et al.* Discovery of N-(3-Carbamoyl-5,5,7,7-tetramethyl-5,7-dihydro-
608 4H-thieno[2,3-c]pyran-2-yl)-IH-pyr azole-5-carboxamide (GLPG1837), a Novel
609 Potentiator Which Can Open Class III Mutant Cystic Fibrosis Transmembrane
610 Conductance Regulator (CFTR) Channels to a High Extent. *J Med Chem* **61**, 1425-1435,
611 doi:10.1021/acs.jmedchem.7b01288 (2018).

612 28 Yeh, H. I., Sohma, Y., Conrath, K. & Hwang, T. C. A common mechanism for CFTR
613 potentiators. *J Gen Physiol* **149**, 1105-1118, doi:10.1085/jgp.201711886 (2017).

614 29 Galietta, L. V., Jayaraman, S. & Verkman, A. S. Cell-based assay for high-throughput
615 quantitative screening of CFTR chloride transport agonists. *Am J Physiol Cell Physiol*
616 **281**, C1734-1742, doi:10.1152/ajpcell.2001.281.5.C1734 (2001).

617 30 Yeh, H. I. *et al.* Identifying the molecular target sites for CFTR potentiators GLPG1837
618 and VX-770. *J Gen Physiol* **151**, 912-928, doi:10.1085/jgp.201912360 (2019).

619 31 Cheng, S. H. *et al.* Defective intracellular transport and processing of CFTR is the
620 molecular basis of most cystic fibrosis. *Cell* **63**, 827-834 (1990).

621 32 Lukacs, G. L. *et al.* The delta F508 mutation decreases the stability of cystic fibrosis
622 transmembrane conductance regulator in the plasma membrane. Determination of
623 functional half-lives on transfected cells. *J Biol Chem* **268**, 21592-21598 (1993).

624 33 Dalemans, W. *et al.* Altered chloride ion channel kinetics associated with the delta F508
625 cystic fibrosis mutation. *Nature* **354**, 526-528, doi:10.1038/354526a0 (1991).
626 34 (2021).

627 35 Fink, C. *et al.* Evaluating the Role of Solubility in Oral Absorption of Poorly Water-
628 Soluble Drugs Using Physiologically-Based Pharmacokinetic Modeling. *Clin Pharmacol
629 Ther* **107**, 650-661, doi:10.1002/cpt.1672 (2020).

630 36 Di, L., Fish, P. V. & Mano, T. Bridging solubility between drug discovery and
631 development. *Drug Discov Today* **17**, 486-495, doi:10.1016/j.drudis.2011.11.007 (2012).

632 37 McCarron, A., Parsons, D. & Donnelley, M. Animal and Cell Culture Models for Cystic
633 Fibrosis: Which Model Is Right for Your Application? *Am J Pathol* **191**, 228-242,
634 doi:10.1016/j.ajpath.2020.10.017 (2021).

635 38 Mysinger, M. M. & Shoichet, B. K. Rapid context-dependent ligand desolvation in
636 molecular docking. *J Chem Inf Model* **50**, 1561-1573, doi:10.1021/ci100214a (2010).

637 39 Wei, B. Q., Baase, W. A., Weaver, L. H., Matthews, B. W. & Shoichet, B. K. A model
638 binding site for testing scoring functions in molecular docking. *J Mol Biol* **322**, 339-355,
639 doi:10.1016/s0022-2836(02)00777-5 (2002).

640 40 Word, J. M., Lovell, S. C., Richardson, J. S. & Richardson, D. C. Asparagine and
641 glutamine: using hydrogen atom contacts in the choice of side-chain amide orientation. *J
642 Mol Biol* **285**, 1735-1747, doi:10.1006/jmbi.1998.2401 (1999).

643 41 Case, D. A. *et al.* AMBER 2015. (2015).

644 42 Gallagher, K. & Sharp, K. Electrostatic contributions to heat capacity changes of DNA-
645 ligand binding. *Biophys J* **75**, 769-776, doi:10.1016/S0006-3495(98)77566-6 (1998).

646 43 Sharp, K. A. Polyelectrolyte electrostatics: Salt dependence, entropic, and enthalpic
647 contributions to free energy in the nonlinear Poisson–Boltzmann model. *Biopolymers* **36**,
648 227-243, doi:10.1002/bip.360360210 (1995).

649 44 Tolmachev, A. *et al.* Expanding Synthesizable Space of Disubstituted 1,2,4-Oxadiazoles.
650 *ACS Combinatorial Science* **18**, 616-624, doi:10.1021/acscombsci.6b00103 (2016).

651 45 Bogolubsky, A. V. *et al.* One-Pot Parallel Synthesis of Alkyl Sulfides, Sulfoxides, and
652 Sulfones. *ACS Combinatorial Science* **17**, 348-354, doi:10.1021/acscombsci.5b00024
653 (2015).

654 46 Bogolubsky, A. V. *et al.* A facile synthesis of unsymmetrical ureas. *Tetrahedron* **67**,
655 3619-3623, doi:<https://doi.org/10.1016/j.tet.2011.03.101> (2011).

656 47 Goehring, A. *et al.* Screening and large-scale expression of membrane proteins in
657 mammalian cells for structural studies. *Nat Protoc* **9**, 2574-2585,
658 doi:10.1038/nprot.2014.173 (2014).

659 48 Zheng, S. Q. *et al.* MotionCor2: anisotropic correction of beam-induced motion for
660 improved cryo-electron microscopy. *Nat Methods* **14**, 331-332, doi:10.1038/nmeth.4193
661 (2017).

662 49 Zhang, K. Gctf: Real-time CTF determination and correction. *J Struct Biol* **193**, 1-12,
663 doi:10.1016/j.jsb.2015.11.003 (2016).

664 50 Scheres, S. H. RELION: implementation of a Bayesian approach to cryo-EM structure
665 determination. *J Struct Biol* **180**, 519-530, doi:10.1016/j.jsb.2012.09.006 (2012).

666 51 Kimanius, D., Forsberg, B. O., Scheres, S. H. & Lindahl, E. Accelerated cryo-EM
667 structure determination with parallelisation using GPUs in RELION-2. *eLife* **5**,
668 doi:10.7554/eLife.18722 (2016).

669 52 Emsley, P., Lohkamp, B., Scott, W. G. & Cowtan, K. Features and development of Coot.
670 *Acta Crystallogr D Biol Crystallogr* **66**, 486-501, doi:10.1107/S0907444910007493
671 (2010).

672 53 Brown, A. *et al.* Tools for macromolecular model building and refinement into electron
673 cryo-microscopy reconstructions. *Acta Crystallogr D Biol Crystallogr* **71**, 136-153,
674 doi:10.1107/S1399004714021683 (2015).

675 54 Murshudov, G. N., Vagin, A. A. & Dodson, E. J. Refinement of macromolecular
676 structures by the maximum-likelihood method. *Acta Crystallogr D Biol Crystallogr* **53**,
677 240-255, doi:10.1107/S0907444996012255 (1997).

678 55 Chen, V. B. *et al.* MolProbity: all-atom structure validation for macromolecular
679 crystallography. *Acta Crystallogr D Biol Crystallogr* **66**, 12-21,
680 doi:10.1107/S0907444909042073 (2010).

681 56 Davis, I. W. *et al.* MolProbity: all-atom contacts and structure validation for proteins and
682 nucleic acids. *Nucleic Acids Res* **35**, W375-383, doi:10.1093/nar/gkm216 (2007).

683 57 Heymann, J. B. & Belnap, D. M. Bsoft: image processing and molecular modeling for
684 electron microscopy. *J Struct Biol* **157**, 3-18, doi:10.1016/j.jsb.2006.06.006 (2007).

685 58 Pettersen, E. F. *et al.* UCSF Chimera--a visualization system for exploratory research
686 and analysis. *J Comput Chem* **25**, 1605-1612, doi:10.1002/jcc.20084 (2004).

687 59 Sondo, E. *et al.* Rescue of the mutant CFTR chloride channel by pharmacological
688 correctors and low temperature analyzed by gene expression profiling. *Am J Physiol Cell
689 Physiol* **301**, C872-885, doi:10.1152/ajpcell.00507.2010 (2011).

690

691 **Acknowledgments**

692 We thank M. Ebrahim and J. Sotiris at Rockefeller's Evelyn Gruss Lipper Cryo-Electron
693 Microscopy Resource Center for assistance in data collection, Yiming Niu and Chen Zhao for
694 help with cryo-EM data processing, and Iris Torres and Bilge Bebek for technical assistance.
695 We would also like to thank Luis J. Galietta for sharing the CFBE41o⁻ cells expressing F508del-
696 CFTR and the fluorescent protein EYFP-H148Q/I152L/F46L.

697

698 **Funding:** This work is supported by the Howard Hughes Medical Institute (to J.C.),
699 R35GM122481 (to B.K.S.), GM133836 (to J.J.I.) and the Deutsche Forschungsgemeinschaft (to
700 P.G.).

701

702 **Author Contributions:** A.L.K. performed molecular docking; F.L., N.S.O, and H.L.P. tested
703 compounds from the initial screen; J.L. carried out majority of the patch-clamp experiments;
704 N.S.O. prepared sample and collected data of the CFTR/853 complex; F.L. determined the
705 structure; I.S.K., Y.S.M., and J.J.I. synthesized the first panel of ligands; S.T., K.D., and J.E.
706 synthesized and chemically characterized new CFTR potentiators and inhibitors. P.G., B.K.S.,
707 and J.C. supervised the study. F.L., A.L.K., J.L., J. E., B.K.S., and J.C. wrote the manuscript
708 with input from all authors.

709

710 **Competing interests:** B.K.S. and P.G. are founders of Epiodyne. B.K.S. is a co-founder of
711 BlueDolphin and of Deep Apple Therapeutics, as is J.J.I., and serves on the SRB of Genentech
712 and on the SABs of Vilya Therapeutics and Umbra Therapeutics, and consults for Great Point
713 Ventures and for Levator Therapeutics. A patent on the discovery of positive and negative
714 allosteric regulators for CFTR has been filed. The authors declare no other competing interests.

715

716

717 **Additional information**

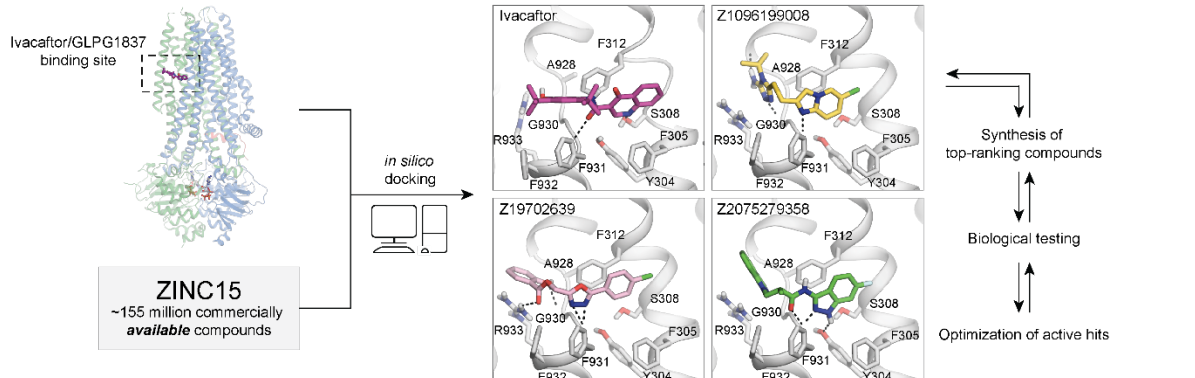
718 Extended data and supplementary information are available for this manuscript.

719

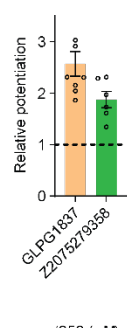
720

Figure 1

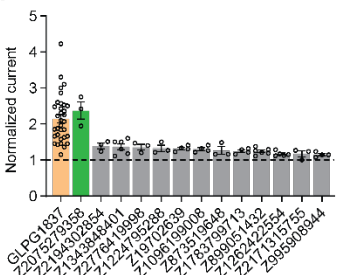
A



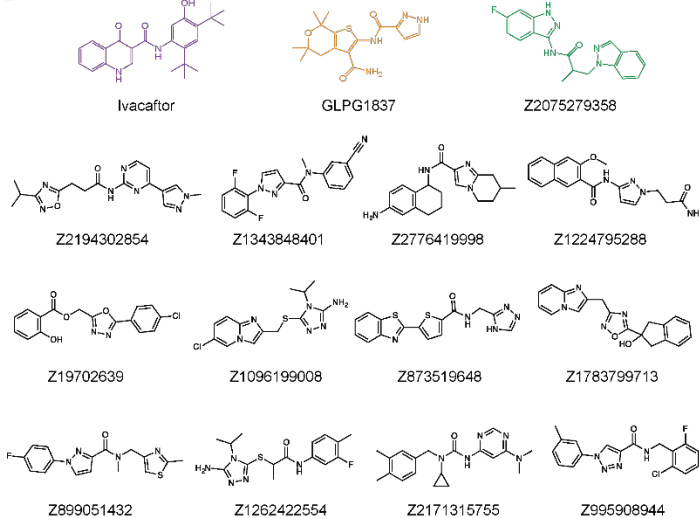
B



C



D



E

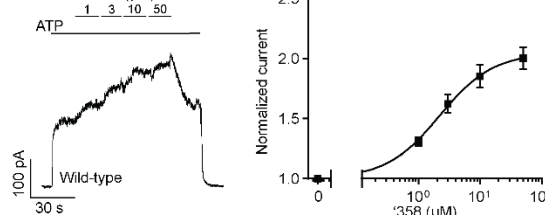


Figure 1: Ultra-large docking screen identifies novel CFTR potentiators. **(a)** The workflow of this study. **(b)** Compound Z2075279358 ('358) potentiates $\Delta F 508$ CFTR. CFBE41o⁻ cells homozygous for $\Delta F 508$ CFTR were treated with 1 μ M lumacaftor and 20 μ M forskolin. The relative potentiation was calculated as the ratio of flux rates with and without potentiator. Data points represent the means and standard errors (SEs) of 6 to 8 measurements (each shown as a dot). **(c)** Potentiation activity of 10 μ M GLPG1837 or 5 μ M compound against WT CFTR fused to a carboxy-terminal GFP tag. Inside-out membrane patches containing WT CFTR were excised from CHO cells and then fully phosphorylated by protein kinase A (PKA) in the presence of 3 mM ATP. The fold stimulation is defined as the ratio of the current in the presence and absence of added compound. Data represent means and SEs of 3-33 patches with individual measurements shown as dots. **(d)** The 2D structures of the potentiators GLPG1837, ivacaftor, and the 13 positive hits from the initial screen. **(e)** Representative macroscopic current trace and dose-response curve of WT CFTR in response to perfusion with '358. CFTR-containing membrane patches were fully phosphorylated by PKA. The current in the presence of 3 mM ATP before titration was used to normalize the current potentiated by different concentrations of '358. The EC_{50} is estimated to be $2.2 \pm 0.6 \mu$ M by fitting the dose-responses with the Hill equation. Data represent means and SEs from 3 patches.

Figure 2

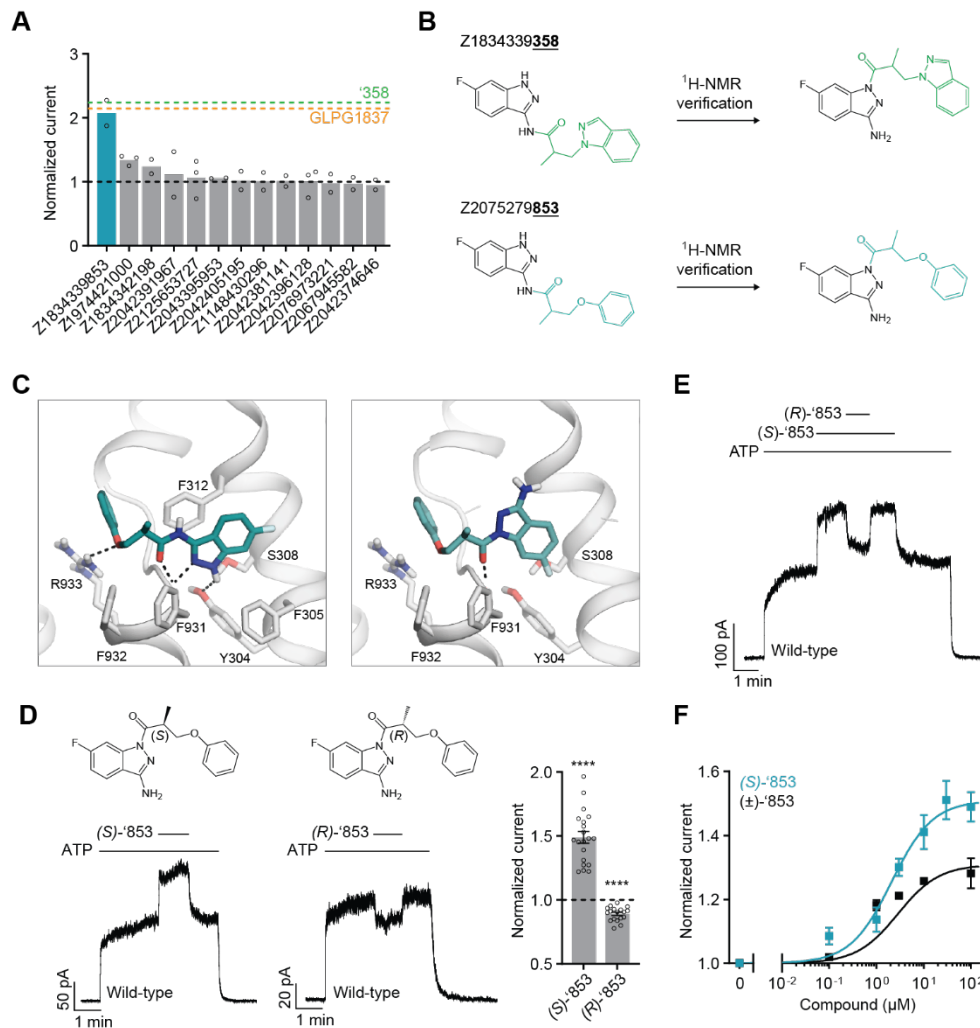


Figure 2: New modulators identified through an analog screen. (a) Potentiation activity of '358' analogs. All compounds were tested at a single concentration of 10 μ M in inside-out membrane patches containing fully phosphorylated WT CFTR. The current stimulation levels of GLPG1837 and '358' are indicated as dashed lines. (b) Reported structures versus the NMR-determined structures. (c) Docked poses of the reported structure of '853' (left) versus the NMR-determined structure of '853' (right). (d) (S)-'853' potentiates WT CFTR currents, while (R)-'853' mildly inhibits them in inside-out patches. Both enantiomers were perfused at 100 μ M concentration. Data represent means and SEs of 20 ((S)-'853) or 18 ((R)-'853) patches. Statistical significance relative to no effect was tested by two-tailed Student's t-test ($****P = 2.3 \times 10^{-9}$ for (S)-'853 and $P = 1.6 \times 10^{-7}$ for (R)-'853). (e) Competition assay showing that the presence of (R)-'853' (100 μ M) diminishes the potentiating effect of (S)-'853' (100 μ M). (f) Dose-response curve of (S)-'853' versus the racemic mixture (\pm)-'853', as described for Figure 1e. The EC_{50} for (S)-'853' was estimated to be $2.1 \pm 0.9 \mu$ M. Data represent means and SEs of 2-20 patches. 3 mM ATP was used in all panels.

Figure 3

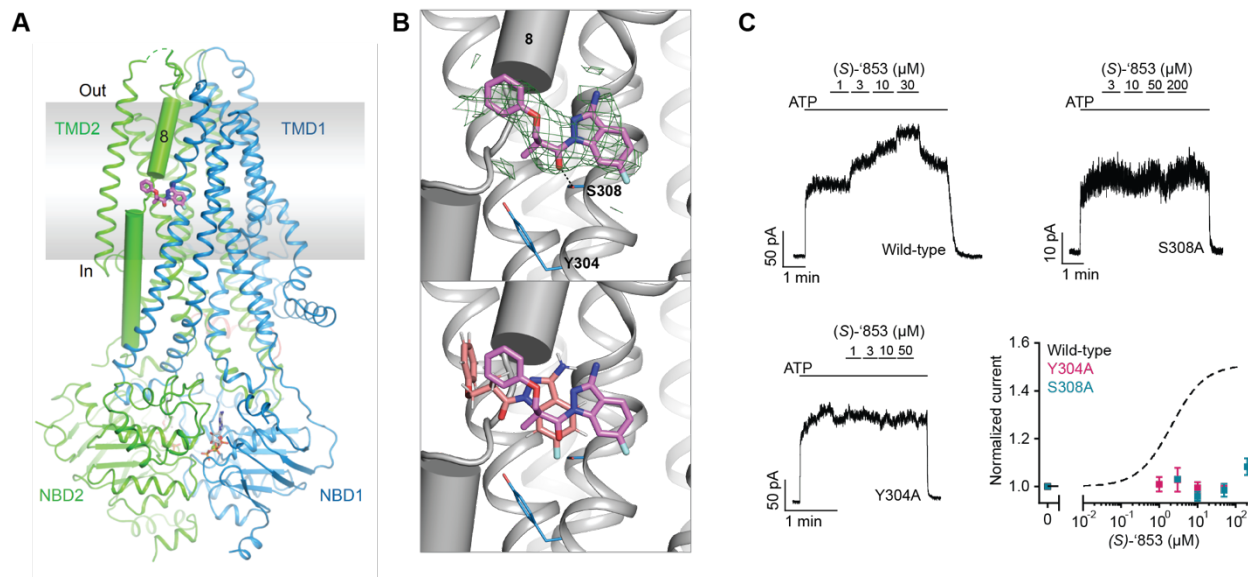


Figure 3: Z1834339853 binds to the same site as ivacaftor and GLPG1837. (a) Cryo-EM structure of phosphorylated and ATP-bound CFTR (E1371Q) in complex with '853. **(b)** Zoomed-in views of the density of '853 (top) and a comparison between the docked pose (salmon) and the cryo-EM pose (magenta). **(c)** Representative macroscopic current traces and dose-response curves of fully phosphorylated WT, S308A, and Y304A CFTR in response to perfusion of (S)-'853 onto inside-out excised membrane patches. 3 mM ATP was used. Each data point represents the mean and SEs determined from 3 to 12 patches.

Figure 4

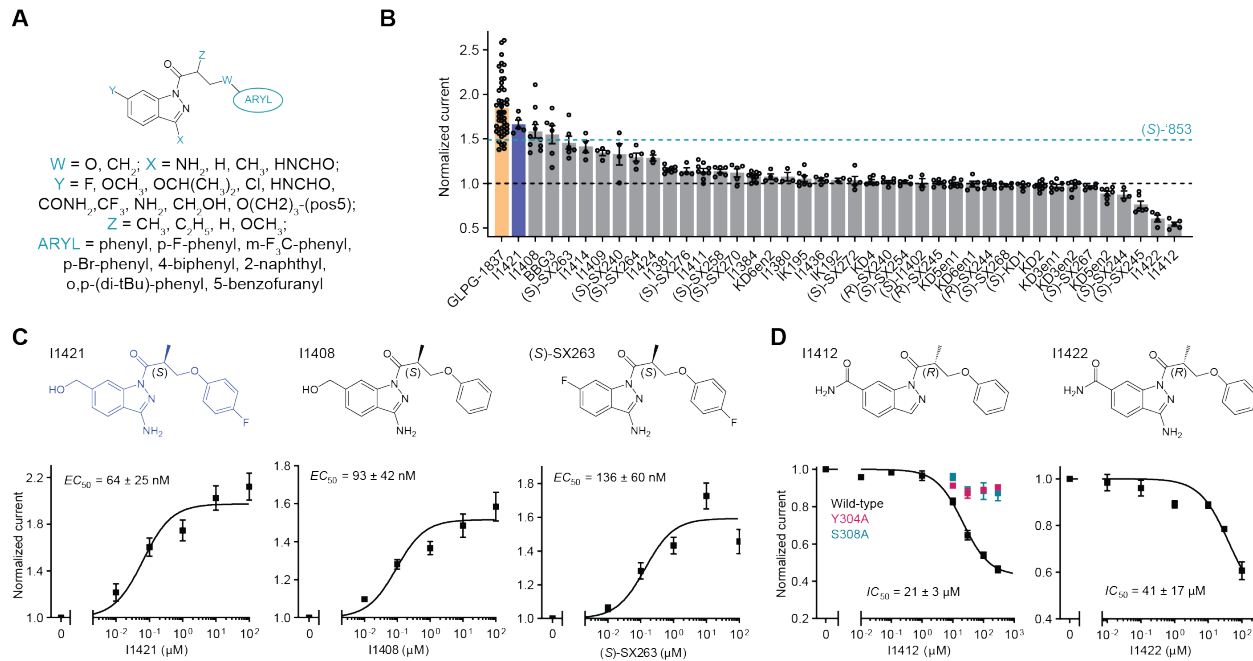


Figure 4: Medicinal chemistry leads to novel CFTR potentiators and inhibitors. (a) General formula of newly synthesized '853 analogs. (b) Effects of '853 analogs on currents measured in inside-out excised membrane patches containing fully phosphorylated WT CFTR. Measurements were made with 3 mM ATP. Data represent means and SEs of 2 to 46 patches. (c) The structures and dose-response curves of three of the most efficacious potentiators. Data represent means and SEs of 5-11 patches. (d) The structures and dose-response curves of the two most efficacious inhibitors. The dose-responses of the Y304A and S308A variants in response to I1412 perfusion were also shown (left). Data represent means and SEs of 2-8 patches.

Figure 5

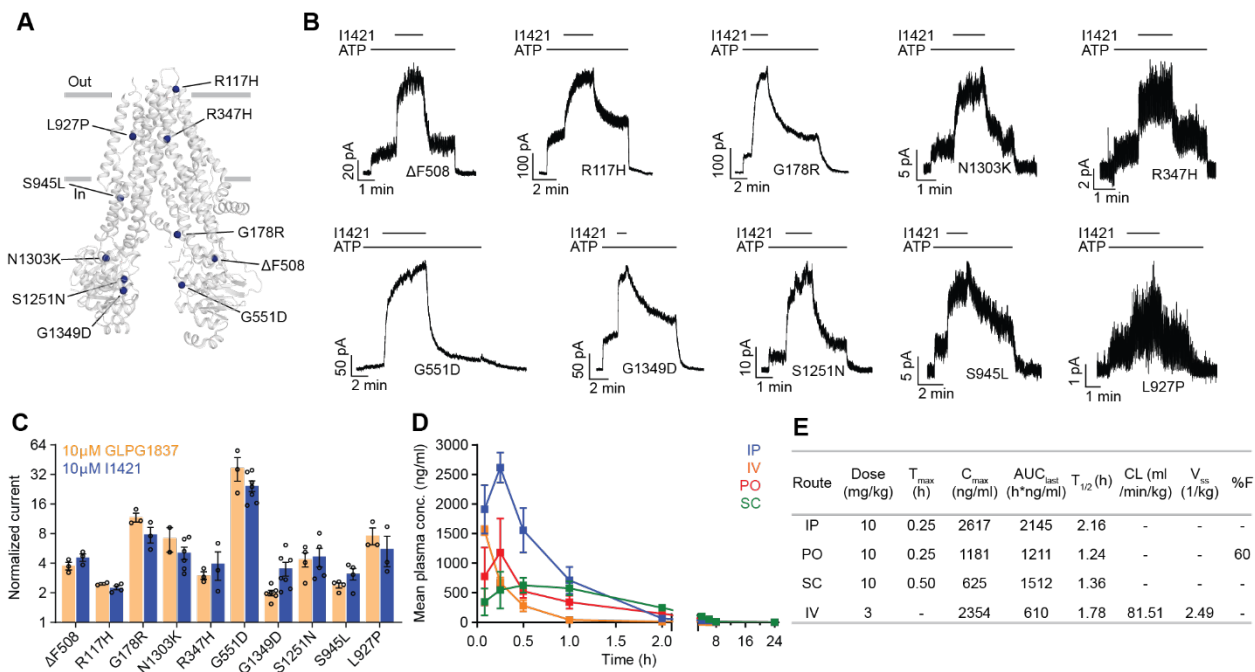
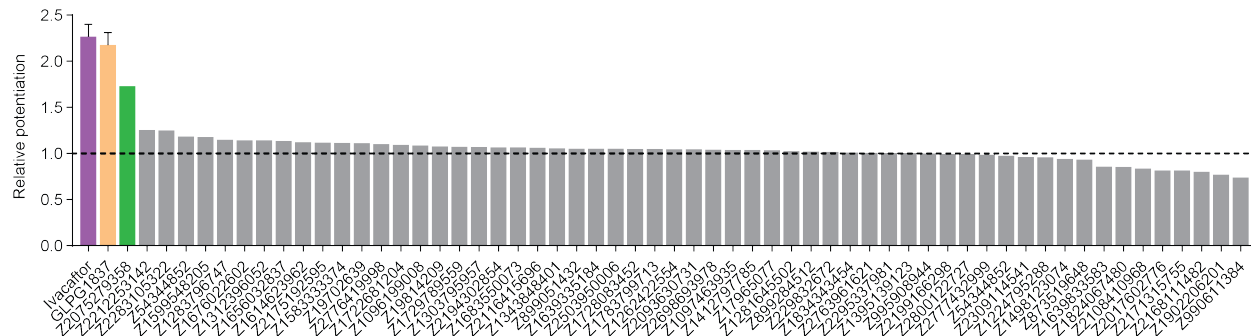
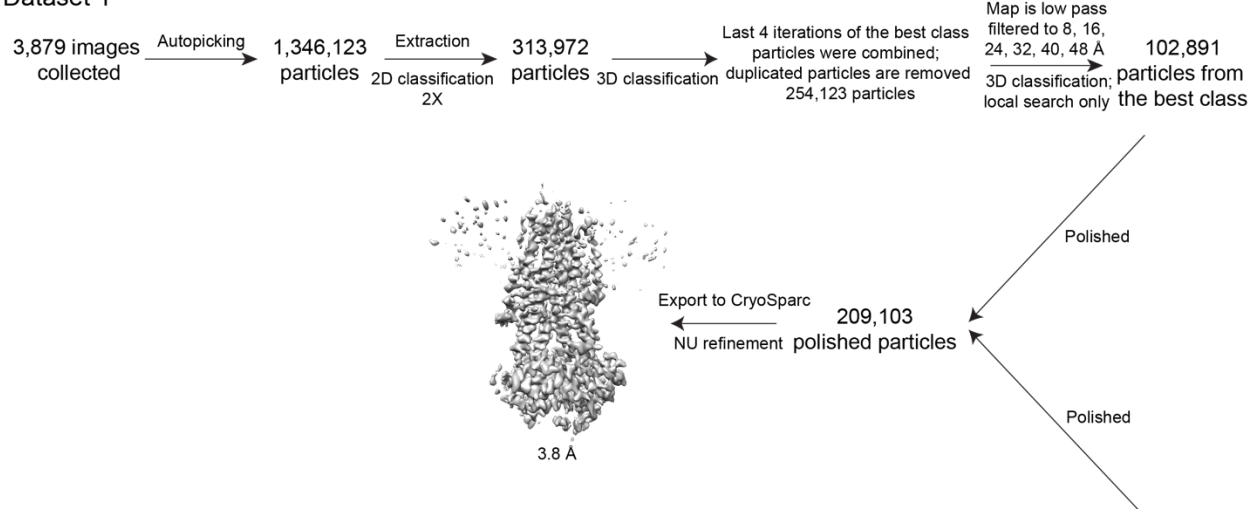


Figure 5: The activity of I1421 against 10 CF-causing mutations. (a) The positions of the mutations mapped onto dephosphorylated and ATP-free CFTR (PDB 5UAK). (b) Representative macroscopic current traces in response to I1421 (10 μ M) perfusion onto inside-out membrane patches excised from CHO cells. 3 mM ATP was used. (c) Potentiation activity of I1421 versus GLPG1837. The mean and SE values were determined from 2 to 7 patches. (d) Pharmacokinetic analysis of compound I1421. Plasma concentration-time profiles in male C57BL/6N mice following a single subcutaneous (SC), intraperitoneal (IP), per-oral (PO) (dose 10 mg/kg) or intravenous (IV) (3 mg/kg) administration. Data represent means and SDs. (e) Selected pharmacokinetic parameters of I1421. C_{max}: peak plasma concentration; T_{max}: the time when the peak plasma concentration was observed; AUC_{last}: the areas under the concentration time curve; T_{1/2}: terminal half-life; CL: clearance, V_{ss}: steady-state volume of distribution; %F: %bioavailability.

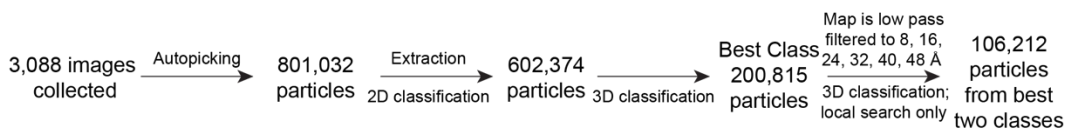


Extended Data Figure 1. Z2075279358 increased the ion flux rate in a bronchial epithelial cell line derived from a patient homozygous for $\Delta F508$ (CFBE410 $^+$ cells expressing $\Delta F508$ -CFTR and the fluorescent protein eYFP-H148Q/I152L/F46L⁵⁹). Cells were treated with 20 μ M forskolin +/- 1 μ M test compound. The relative potentiation was calculated as the ratio of flux rates with and without compound. Data points represent a single measurement for each test compound. For ivacaftor and GLPG1837 data represent means and SEs for 9 or 2 measurements, respectively.

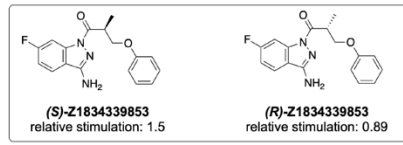
Dataset 1



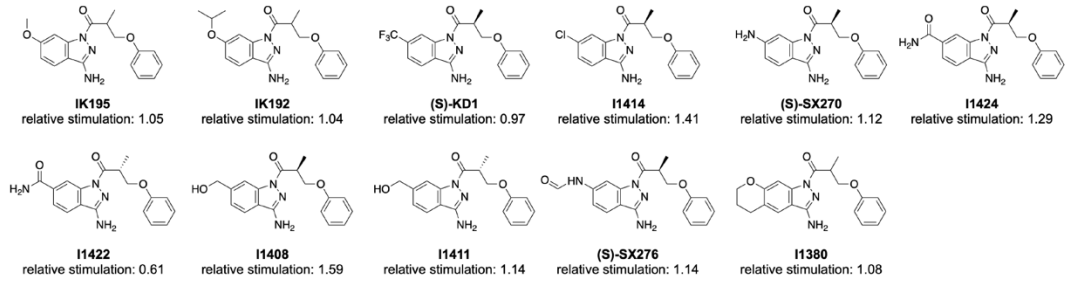
Dataset 2



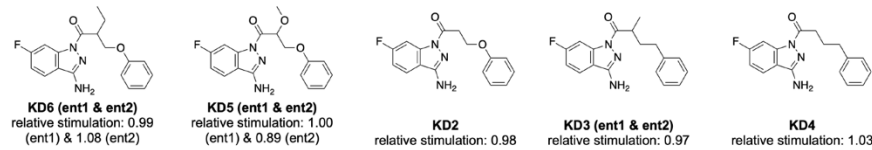
Extended Data Figure 2. Cryo-EM reconstructions of the CFTR-'853 complex. Summary of the image processing procedure.



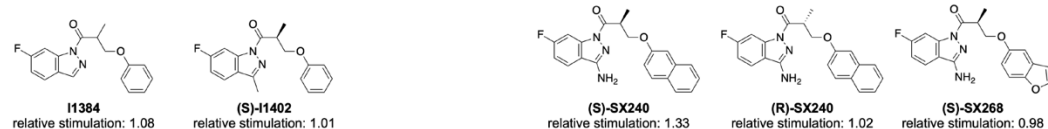
(1) Replacing the fluorine with a larger side chain



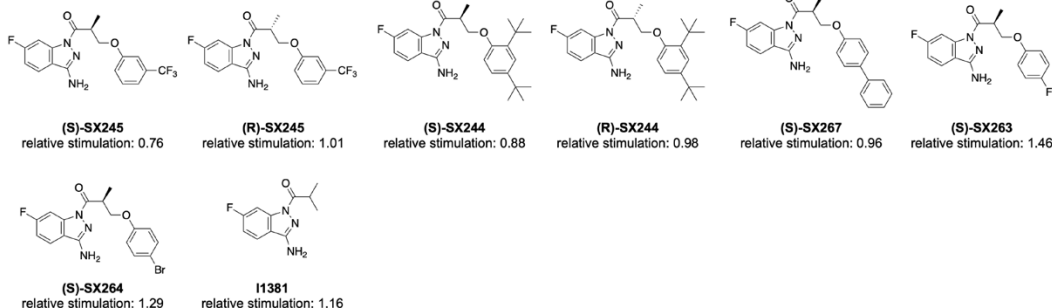
(2) Modification to the linker



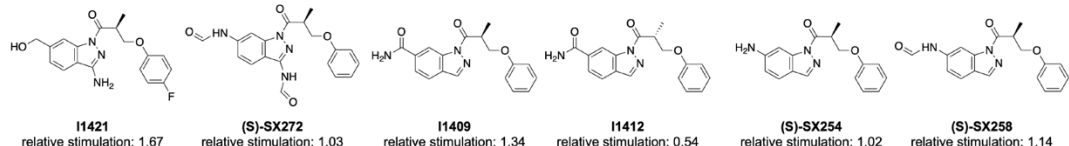
(3) Removing the amino group's hydrogen donor functionality



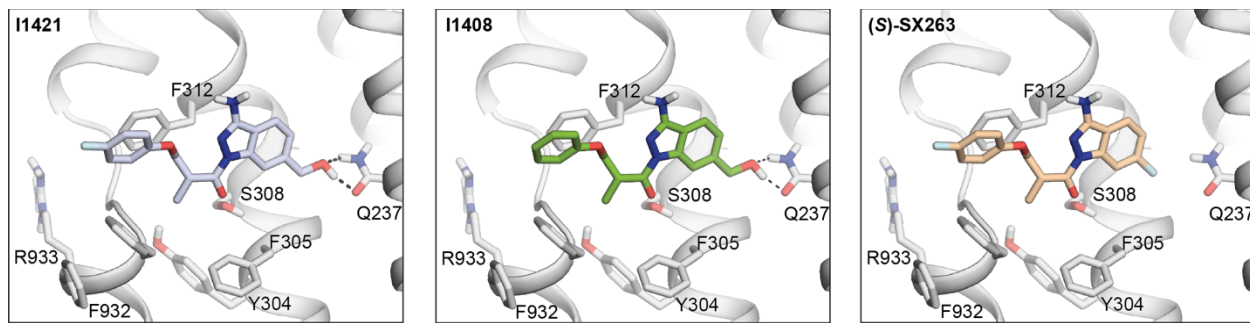
(5) Modification to the phenyl ring



(6) More than one modification



Extended Data Figure 3. SAR for optimization of compound '853.



Extended Data Figure 4. Docked poses of I1421, I1408, and (S)-SX263.

Extended Data Table 1. Potentiating activities of the 13 CFTR primary hits.

Extended Data Table 2. Summary of EM data and structure refinement statistics for CFTR in complex with '853.

Data collection	
Microscope	Titan Krios (FEI)
Voltage (kV)	300
Detector	K2 Summit (Gatan)
Pixel size (Å)	1.03
Defocus range (μm)	1 to 2.5
Movies	6,967
Frames/movie	50
Dose rate (electrons/pixel/s)	8
Total dose (electrons/Å ²)	75
Number of particles	1,948,497
Model composition	
Non-hydrogen atoms	9,682
Protein residues	1,035
Lipids	5
ATP	2
Mg	2
Refinement	
Resolution (Å)	3.8
Sharpening B-factor (Å ²)	-117
RMS deviations	
Bond lengths (Å)	0.005
Bond angles (°)	0.863
Validation	
Molprobity score	2.09
Clashscore, all atoms	16
Favored rotamers (%)	99.9
Ramachandran plot (%)	
Favored	94.87
Allowed	5.13
Outliers	0.0
